RAPID COMMUNICATIONS

PHYSICAL REVIEW C VOLUME 52, NUMBER 6 DECEMBER 1995

# Quantitative description of superdeformed bands with the projected shell model

Yang Sun [1,2,3] and Mike Guidry [2,3]

[1] *Joint Institute for Heavy Ion Research, Oak Ridge National Laboratory, Oak Ridge, Tennessee 37831*

[2] *Department of Physics and Astronomy, University of Tennessee, Knoxville, Tennessee 37996*

*3Physics Division, Oak Ridge National Laboratory, Oak Ridge, Tennessee 37831*

(Received 27 April 1995 )

We propose a theoretical description of superdeformed bands based on the projected shell model. The shell model basis is constructed at the superdeformed minimum and projected onto states of good angular momentum, and a two-body Hamiltonian is then diagonalized in this basis. We take the superdeformed band in $^{132}$Ce as an example. Good agreement with the measured gamma-ray energies allows us to suggest spin values for these superdeformed states. Finally, we propose an explanation for the recently observed $\Delta I=4$ bifurcation disappearance at a rotational frequency of $\hbar\omega\simeq 0.65$ in this nucleus.

PACS number(s): 21.10.Re, 21.60.Cs, 27.60.+j

The topic of superdeformation (SD) has been at the forefront of nuclear structure physics since the observation of the SD band in $^{152}$Dy [1]. The existence of enhanced deformation, diminished pairing, and less frequent band crossings makes phenomena such as identical bands [2] and $\Delta I=4$ bifurcation [3] easier to detect in SD than in normally deformed (ND) systems.

Superdeformation is both theoretically and experimentally a well-established concept, but the measured SD bands are not firmly tied to the nuclear ground state by complete decay sequences. Thus, the spin assignments for superdeformed states remain uncertain. This leaves hypotheses such as the existence of quantized alignment [4] open questions [5]. Other important physical quantities such as the static moment of inertia $\mathcal{J}^{(1)}$ for SD bands cannot be uniquely determined because one does not know the angular momenta. Mean-field descriptions of the cranking type are of limited utility for these questions because angular momentum is not a conserved quantity in those theories.

In this paper we propose a description of SD bands based on the projected shell model (PSM) [6,7]. The PSM is a shell model truncated in a deformed (Nilsson-type) single particle basis, with pairing correlations incorporated into the basis by a BCS calculation for the Nilsson states. More precisely, the truncation is first implemented in the multi-quasiparticle basis with respect to the deformed BCS vacuum $|\phi\rangle$ [see Eq. (1) below]; then the violation of rotational symmetry is removed by projection [8] to form a shell model basis in the laboratory frame. Finally a shell model Hamiltonian is diagonalized in this projected space. For this study we include 0-, 2-, and 4-quasiparticle (qp) states:

$$\{|\phi\rangle, \alpha^\dagger_{n_i}\alpha^\dagger_{n_j}|\phi\rangle, \alpha^\dagger_{p_k}\alpha^\dagger_{p_l}|\phi\rangle, \alpha^\dagger_{n_i}\alpha^\dagger_{n_j}\alpha^\dagger_{p_k}\alpha^\dagger_{p_l}|\phi\rangle\}, \quad (1)$$

where $\alpha^\dagger$ is the creation operator for a quasiparticle and the index $n$ ($p$) denotes neutrons (protons). Thus, the PSM enjoys many of the advantages of standard mean-field theories in that it can easily account for the most important nuclear correlations (the pairing and quadrupole interactions), and that the results can be interpreted in simple physical terms. However, the PSM goes beyond the mean field because it incorporates shell-model configuration mixing within the basis of projected states.

The model was initially constructed to treat normally deformed high-spin states [6], and has proven to be rather successful [7,9] in this application. Application of this model to superdeformation requires an assignment for the interaction terms of the two-body Hamiltonian. Although there is no reason of principle to expect that these interaction strengths will be the same as those found to be appropriate for normal deformation, in this paper we take a minimalist approach: we attempt to calculate the properties of SD states using the same Hamiltonian as employed for the ND case. The Nilsson parameters are well established for the normal deformation region and are simply extrapolated to the larger deformation region. We have applied these methods systematically to the SD states in the mass-130 region. In this paper we shall report on results obtained for $^{132}$Ce as a representative example of these calculations. This is a typical SD nucleus in the $A=130$ mass region and has been studied in a variety of experimental [10–13] and theoretical [14] papers. Calculations for SD bands in other mass regions are underway and will be reported in forthcoming publications.

We use the "$Q\times Q$ plus monopole pairing plus quadrupole pairing force" Hamiltonian [6,7]

$$\hat{H}=\hat{H}_0-\frac{\chi}{2}\sum_\mu \hat{Q}^\dagger_\mu\hat{Q}_\mu-G_M\hat{P}^\dagger\hat{P}-G_Q\sum_\mu \hat{P}^\dagger_\mu\hat{P}_\mu, \quad (2)$$

which has been used to explain the systematics of rotational spectra for a large number of nuclei. In Eq. (2), the first term $\hat{H}_0$ is the spherical single-particle Hamiltonian and the remaining terms are residual quadrupole-quadrupole, monopole pairing, and quadrupole pairing interactions, respectively.

The quasiparticle states in Eq. (1) are determined by the following procedure: For the Nilsson parameters $\kappa$ and $\mu$ we take the $N$-dependent values from Ref. [15], subject to modifications introduced by Ref. [16]. The deformation parameter $\epsilon_2$ in the Nilsson model is a well-studied quantity for this nucleus. Instead of deriving it from self-consistent mean-field calculations [14], we consider it to be known and use a

 

value $\epsilon_2 = 0.38$. This is the value obtained by minimizing the single particle energy [14] and is consistent with the experimental value [11]. The strength of the $\hat{Q}^\dagger\hat{Q}$ force in Eq. (2) was then fixed in such a way that it would give the empirical deformation in the mean-field calculations, and the qp representation was then defined by applying the BCS procedure to the Nilsson basis. We note that the exact choice of deformation parameter is not as crucial in our shell model approach as they would be in a mean-field approach because it is only used to construct a basis. The final results come from diagonalizing a two-body Hamiltonian in this basis, and therefore incorporate fluctuations beyond the average deformation and pairing fields.

The single-particle basis in the PSM calculation consisted of three major shells each for neutrons and protons. For the mass region $A \sim 130$, $N = 3$, 4, and 5 shells were employed for the protons in both the ND and the SD cases. For neutrons we used $N = 3$, 4, and 5 for the ND case and $N=4$, 5, and 6 for the SD case. These valence space choices for the superdeformed case incorporate high-$N$ shells thought to be important for the SD moment of inertia [17]. The strength of the monopole pairing interaction in Eq. (2) is critical for a quantitative discussion of the moment of inertia. As was recognized long ago [18], the pairing strength is a function of the size of the single-particle space that is employed, and decreases roughly as the inverse square root of the number of levels participating in the BCS correlations. We employ monopole pairing strengths

$$G_M^n(\mathrm{ND}) = \left[19.6 - 15.7\,\frac{N-Z}{A}\right] \times A^{-1},$$

$$G_M^n(\mathrm{SD}) = \left[18.0 - 14.4\,\frac{N-Z}{A}\right] \times A^{-1}, \qquad (3)$$

$$G_M^p(\mathrm{ND,\ SD}) = 19.6 \times A^{-1},$$

which are the strengths found to be appropriate for this mass region in Ref. [19], but scaled according to the above considerations to account for the different spaces employed here and in Ref. [19]. (A similar prescription was used in Ref. [20].) However, we do not claim that our present choice of the strengths of Eq. (3) are optimal since we did not try to fit many samples. Finally, the quadrupole pairing strength $G_Q$ in Eq. (2) is assumed to be 16% of the monopole pairing $G_M$, in agreement with the average ratio of quadrupole to monopole pairing strengths found to be appropriate for normally deformed rare-earth nuclei [7,9].

Our results are compared with the data [13] in Fig. 1, where the dynamical moment of inertia $\mathfrak{I}^{(2)}$ is plotted as function of rotational frequency $\hbar\omega$. The peak appearing at $\hbar\omega \simeq 0.36$ corresponds to a near-simultaneous crossing of four bands: the SD ground-state band ($g$ band), a band associated with the alignment of a $\nu i_{13/2}$ neutron pair, and two bands corresponding to $h_{11/2}$ proton alignment (see Fig. 2 for their configurations). The neutron pair consists of the $K = 1/2$ and $K = 3/2$ quasineutrons coupled to $K = 1$. Because of the strong decoupling effect, this 2-quasineutron state becomes yrast after the crossing with the $g$ band. The two quasiproton bands rise quickly away from yrast, as we discuss further below, and so play a minor role in the structure

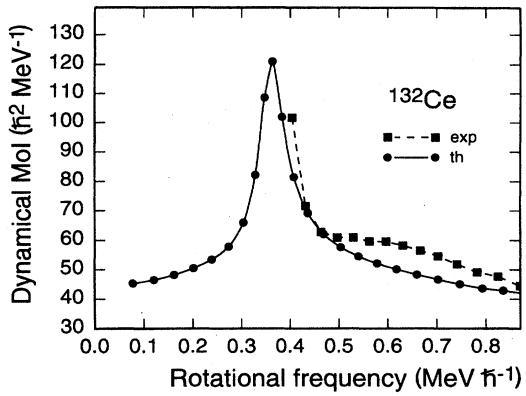


FIG. 1. Comparison of calculated SD dynamical moment of inertia $\mathfrak{I}^{(2)}$ ($\hbar^2$ MeV$^{-1}$) with the data [13]. Definitions of the quantities: $\mathfrak{I}^{(2)} = 4/[E_\gamma(I) - E_\gamma(I-2)]$, $\hbar\omega = E_\gamma(I)/2$, and $E_\gamma(I) = E(I) - E(I-2)$.

of the presently known yrast sequence in this nucleus. However, the proton bands may play a significant role in the rapid disappearance of superdeformed population observed near this band crossing, and in the yrast structure of adjacent odd-neutron nuclei where the neutron alignment is blocked (see below).

For a better understanding of these results let us now look at the band diagram shown in Fig. 2. A band diagram is defined [7] as the diagonal elements of the Hamiltonian in the projected basis of Eq. (1). We concentrate on two kinds

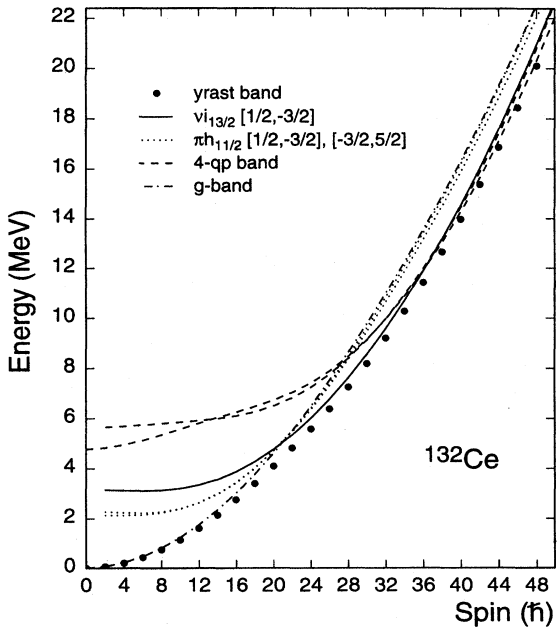


FIG. 2. Band diagram (bands before configuration mixing) and the yrast band (the lowest band after configuration mixing, denoted by dots). Only the lowest-lying bands in each configuration are shown. For the 2-qp states, $K$ quantum numbers are given in square brackets. The 4-qp states are combinations of one 2-quasineutron and one 2-quasiproton bands shown in this figure.

of band crossings: the first crossing between the $g$ band and the 2-qp bands at spin $22\hbar$, and the second crossing between the 2-qp and the 4-qp bands at spin $38\hbar$. The gain of alignment can be read from the plot. In this energy vs angular momentum plot, rotational frequency $\omega = dE/dI$ is the slope of the curve. For the 2-quasineutron band one finds that $\omega \simeq 0$ until the system begins to rotate at spin $12\hbar$ (see the flat portion of the curve in Fig. 2). This is a perfect alignment process, since $12\hbar$ is the maximum angular momentum that a pair of $j = 13/2$ particles can contribute. The same perfect alignment can be seen for $h_{11/2}$ proton pairs, which do not rotate until spin $10\hbar$. Thus, for a 4-qp configuration (2-quasineutron + 2-quasiproton), the band begins to approximate collective rotational motion near $22\hbar = 12\hbar + 10\hbar$.

As noted above, the 2-quasineutron band and two 2-quasiproton bands cross the $g$ band at almost the same point (spin $22\hbar$). Therefore, the band interaction at the first crossing involves many bands. Because of different rotational frequencies, the proton bands depart quickly from the yrast region with increasing angular momentum and are less likely to be detected experimentally. In a separate publication [21] we shall demonstrate that the present methods give a satisfactory description of odd-mass superdeformed bands in this mass region with the same parameter set employed for even-mass nuclei. These calculations indicate that this proton band crossing is dominant in the odd-neutron case (e.g., $^{131}$Ce), where the neutron crossing is blocked, and that the effect of this crossing is less pronounced than that of the neutron crossing because of the smaller crossing angle associated with the proton alignments (see Fig. 2). This explains the observed differences in dynamical moment of inertia between, for example, $^{131}$Ce and $^{132}$Ce at rotational frequencies near $\hbar\omega \simeq 0.40$. We find that bands with alignment of neutron pairs built upon $h_{9/2}$ and $h_{11/2}$ orbitals lie high in energy (more than 1 MeV higher than the 2-qp bands presented here at the crossing spin $22\hbar$) and are unlikely to play a significant role in the yrast region, which is contrary to the results of Ref. [14].

The neutron band remains the yrast band until it crosses with 4-qp states at spin $38\hbar$. Thus, the observed yrast band in this spin region is mainly 2-quasineutron in structure, as indicated in Fig. 2. After the second band crossing, the yrast band structure is dominated by 4-qp components. This second crossing has not entered other theoretical [14] and experimental [11] discussions, probably because its effect on the observed bands is small. Indeed, even in the plot of the dynamical moment of inertia shown in Fig. 1, one can hardly see the effect. The crossing partners approach each other, interact, and move away with very similar behavior (i.e., with very small crossing angle [7]) as if no crossing had occurred as far as the moment of inertia diagram is concerned. However, such a crossing implies a rearrangment of the wave function at that spin for the yrast structure and should have other observable consequences. We will suggest below that the second band crossing plays an important role in understanding the observed anomalous behavior of $\Delta I = 4$ bifurcation in $^{132}$Ce [13].

We observe that all the configurations (0-, 2-, and 4-qp states) shown in Fig. 2 behave similarly at higher spins: above angular momentum $36\hbar$, all bands displayed are approximately parallel (they rotate with the same frequency).

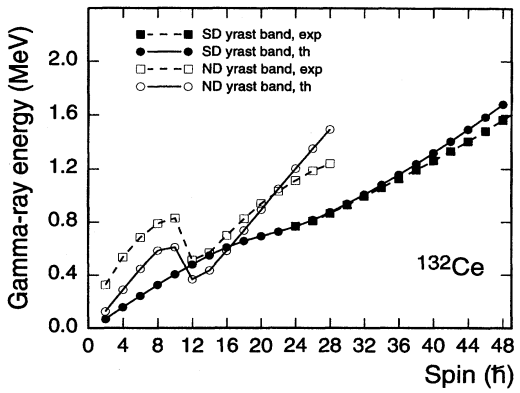


FIG. 3. Comparison of the calculated gamma-ray energy with the data (SD taken from [13] and ND from [22]). $E_\gamma(I)$ is defined as $E(I) - E(I-2)$.

Higher band crossings (e.g., 6-qp with 4-qp states) may occur at higher spins ($>50\hbar$), but with even smaller crossing angles. Therefore, the effects caused by such crossings on the moment of inertia should be smaller still.

The good agreement with data encourages us to make a theoretical spin assignment for the observed SD band in $^{132}$Ce. In Fig. 3 we plot the gamma-ray energy $E_\gamma$ as a function of spin $I$. For comparison, the ND yrast band of the same nucleus is also plotted. The ND calculation is carried out in such a way that the shell model space is now truncated at a deformation of $\epsilon_2 = 0.21$, with a corresponding change in the strength of the quadrupole-quadrupole term in Eq. (2) according to the deformation self-consistency condition discussed above. For the SD band, the calculation coincides best with the data when we place the measured [13] first gamma-ray energy at spin $24\hbar$. This is a positive shift of $6\hbar$ relative to the spin assignment given in Refs. [11,23]. The upper portion of the theoretical SD curve deviates slightly from the experimental curve, suggesting that 6-qp states may be required in the projected space of Eq. (1) to describe the highest spins accurately .

A detailed analysis of the SD data indicates an interesting staggering for $\Delta I = 2$ spin members in some SD bands [3]. This $\Delta I = 4$ *bifurcation effect* suggests a possible fourfold rotational symmetry of the nuclear shape. However, we have shown recently [24] that the PSM can produce $\Delta I = 4$ bifurcation through the usual interactions, without introducing an explicit fourfold symmetry into the Hamiltonian. In future work we will address whether the PSM can describe the detailed features of $\Delta I = 4$ bifurcation observed in superdeformed nuclei, but we would like to conclude this paper by giving a possible cause for a particular aspect of this phenomenon: the as-yet unexplained observation that in $^{132}$Ce the energy staggering starts at low rotational frequency, dies away to zero near $\hbar\omega \simeq 0.65$, and reappears at higher frequency with no change in phase [13]. Our calculation shows that the second band crossing occurs at spin $38\hbar$ (see Fig. 2), which corresponds exactly to $\hbar\omega \simeq 0.65$. We suggest that this crossing leads to the modulation in the staggering behavior. As already pointed out, the crossing angle is so small that one cannot see the effect of this crossing in the $\mathcal{I}^{(2)}$ diagram

(see Fig. 1). Thus, we conclude that the $\Delta I=4$ bifurcation amplitude may be a sensitive probe of high-spin superdeformed band crossings in a regime where such crossings may have little obvious influence on the dynamical moment of inertia.

In summary, we have presented the first calculations of superdeformed bands using the projected shell model. The results shown here are representative of a set of calculations that we have performed indicating that this method gives a quantitative description of observed superdeformed bands in the mass-130 region, with parameters specified by a prescription analogous to that used for normally deformed states. Although we certainly expect that optimal parameters for superdeformed systems will differ from those for normally deformed systems, the present results with a nonoptimized set of parameters are already extremely encouraging. Thus, the PSM could be a powerful tool for the systematic analysis of superdeformed data. Because our theory conserves angular momentum we are able to make theoretical spin assignments for superdeformed bands. For the presently employed interaction strengths, our angular momentum assignments for states in $^{132}$Ce are 6 units higher than those assigned by the experimental discoverers of the band. We find a complex intersection of four bands at the point where the superdeformed band in $^{132}$Ce is known to exhibit anomalies in the moment of inertia and to lose intensity rapidly, and find that the three 2-qp bands crossing the ground band at this point correspond to structures that are fully aligned before they begin to rotate. These findings may be relevant to the superdeformed feeding-out mechanism, though we have not addressed that issue explicitly in this paper. Finally, we suggest that the recently discovered modulation of the $\Delta I=4$ bifurcation to zero near a frequency of $\hbar\omega\simeq 0.65$ in $^{132}$Ce is a consequence of a band crossing observed at this frequency that has little influence on the dynamical moment of inertia plot. Thus, we propose that fine structure in the $\Delta I=4$ bifurctation effect may be a sensitive fingerprint of high-spin band crossings that might escape detection in a simple moment-of-inertia analysis.

Finally, we would like to stress that the PSM may be superior to the traditional cranking model analysis of superdeformed data in certain respects. The PSM restores quantum numbers violated in mean-field calculations, thus ensuring that band mixing is carried out at a fixed angular momentum rather than a fixed rotational frequency. The resulting theory should be more reliable in the band-crossing region. Although we have not done so here, a corresponding restoration of particle number symmetry can also be implemented with these methods. More importantly, the PSM implements shell-model configuration mixing by diagonalization of a two-body Hamiltonian in the projected space. The Nilsson plus BCS single quasiparticle states serve only as a basis from which a more sophisticated wave function is constructed. Important correlations that are omitted at the mean-field level are included by such configuration mixing. Furthermore, the laboratory-system wave functions obtained from the PSM can be used directly to compute transition probabilities, unlike the situation with wave functions of the cranking type. A fast and easily used computer code is available from the authors that implements these features of the PSM. We believe that such a code will be of considerable utility in analyzing the data emerging from the large new detector arrays.

Discussions with C.-L. Wu, W. Nazarewicz, and J.-y. Zhang are acknowledged, and we thank A. T. Semple *et al.* for communicating experimental results prior to publication. The Joint Institute for Heavy Ion Research has as member institutions the University of Tennessee, Vanderbilt University, and the Oak Ridge National Laboratory; it is supported by the member institutions and by the U.S. Department of Energy through Contract No. DE-AS05-76ER04936 with the University of Tennessee. Theoretical nuclear physics research at the University of Tennessee is supported by the U.S. Department of Energy through Contract No. DE-FG05-93ER40770. Oak Ridge National Laboratory is managed by Lockheed Martin Energy Systems, Inc., for the U.S. Department of Energy under Contract No. DE-AC05-84OR21400.

[1] P.J. Twin *et al.*, Phys. Rev. Lett. **57**, 811 (1986).
[2] T. Byrski *et al.*, Phys. Rev. Lett. **64**, 1650 (1990).
[3] S. Flibotte *et al.*, Phys. Rev. Lett. **71**, 4299 (1993).
[4] F.S. Stephens *et al.*, Phys. Rev. Lett. **65**, 301 (1990).
[5] C.-L. Wu, D.H. Feng, and M. Guidry, Phys. Rev. Lett. **66**, 1377 (1991); Phys. Rev. C **46**, 1339 (1992).
[6] K. Hara and S. Iwasaki, Nucl. Phys. **A348**, 200 (1980).
[7] K. Hara and Y. Sun, Nucl. Phys. **A529**, 445 (1991).
[8] P. Ring and P. Schuck, *The Nuclear Many Body Problem* (Springer-Verlag, New York, 1980).
[9] K. Hara and Y. Sun, Nucl. Phys. **A531**, 221 (1991); **A537**, 77 (1992); Y. Sun and J.L. Egido, *ibid.* **A580**, 1 (1994); Phys. Rev. C **50**, 1893 (1994).
[10] P.J. Nolan *et al.*, J. Phys. G **11**, L17 (1985).
[11] A.J. Kirwan *et al.*, Phys. Rev. Lett. **58**, 467 (1987).
[12] D. Santos *et al.*, Phys. Rev. Lett. **74**, 1708 (1995).
[13] A.T. Semple *et al.*, submitted to Phys. Rev. Lett.
[14] R. Wyss, J. Nyberg, A. Johnson, R. Bengtsson, and W. Nazarewicz, Phys. Lett. B **215**, 211 (1988).
[15] T. Bengtsson and I. Ragnarsson, Nucl. Phys. **A436**, 14 (1985).
[16] J.-y. Zhang, N. Xu, D.B. Fossan, Y. Liang, R. Ma, and E.S. Paul, Phys. Rev. C **39**, 714 (1989).
[17] T. Bengtsson, I. Ragnarsson, and S. Åberg, Phys. Lett. B **208**, 39 (1988).
[18] Z. Szymański, Nucl. Phys. **28**, 63 (1961).
[19] W. Dietrich, A. Bäcklin, C.O. Lannergård, and I. Ragnarsson, Nucl. Phys. **A253**, 429 (1975).
[20] S. Iwasaki, Prog. Theor. Phys. **79**, 730 (1988).
[21] Y. Sun *et al.* (unpublished).
[22] Yu.V. Sergeenkov, Nucl. Data Sheets **65**, 301 (1992).
[23] X.-L. Han and C.-L. Wu, At. Data Nucl. Data Tables **52**, 43 (1992).
[24] Y. Sun, J.-y. Zhang, and M.W. Guidry, Phys. Rev. Lett. **75**, 3398 (1995).